Texture and structural refinement using neutron diffraction data from molybdite (MoO_3) and calcite ($CaCO_3$) powders and a Ni-rich $Ni_{50.7}Ti_{49.30}$ alloy

Husin Sitepu[a)]
Crystallography Laboratory, Virginia Tech, Blacksburg, Virginia 24061

(Received 9 March 2009; accepted 1 August 2009)

Preferred orientation or texture is a common feature of experimental powder patterns. The mathematics of two commonly used models for preferred orientation—the March-Dollase and the generalized spherical-harmonic models—is reviewed. Both models were applied individually to neutron powder data from uniaxially pressed molybdite (MoO_3) and calcite ($CaCO_3$) powders in Rietveld analyses, as well as the as-received powders. The structural refinement results are compared to single-crystal structures. The results indicate that reasonable refinement of crystal structures can be obtained using either the March model or generalized spherical-harmonic description. However, the generalized spherical-harmonic description provided better Rietveld fits than the March model for the molybdite and calcite. Therefore, the generalized spherical-harmonic description is recommended for correction of preferred orientation in neutron diffraction analysis for both crystal structure refinement and phase composition analysis. Subsequently, the generalized spherical-harmonic description is extended to crystal structure refinement of annealed and the aged polycrystalline Ni-rich $Ni_{50.7}Ti_{49.30}$ shape memory alloys. © *2009 International Centre for Diffraction Data.* [DOI: 10.1154/1.3257906]

Key words: preferred orientation, texture, neutron powder diffraction, March model, generalized spherical harmonics, molybdite, calcite, $Ti_{50.70}Ni_{49.30}$ shape memory alloy

I. INTRODUCTION

As a consequence of the preparation technique or the habit of the crystallites, crystallographic preferred orientation (PO) or texture is an important problem in powder diffraction studies because it can cause serious systematic errors in crystal structure refinement and phase composition analysis. Initially, Rietveld (1969) used a simple Gaussian model to describe grain orientations in neutron powder diffraction (ND) data. [Rietveld analysis adjusts the refinable parameters until the best fit of the entire calculated pattern to the entire measured pattern is achieved. Additionally, the refined atomic parameters should agree well with the structure derived from single-crystal X-ray diffraction data.] Since then, preferred orientation has been a part of Rietveld refinement because the method is well suited to low-symmetry compounds with many closely spaced and partially overlapped peaks, whereas it is still difficult to measure quantitative pole figures for complex X-ray powder diffraction (XRD) and ND data for such materials. The March model (Dollase, 1986; O'Connor *et al.*, 1991, 1992; Sitepu, 1991, 1998, 2002; Sitepu, O'Connor, and Li, 2004, 2005), the generalized spherical-harmonic (GSH) description (Ahtee *et al.*, 1989; Popa, 1992; Järvinen, 1993; Von Dreele, 1997; Bergmann *et al.*, 2001; Sitepu *et al.*, 2001; Sitepu, Schmahl, and Allafi *et al.*, 2002; Sitepu, Schmahl, and Stalick, 2002; Sitepu, Schmahl, and Von Dreele, 2002; Sitepu, 2003, 2007, 2008; Sitepu, O'Connor, Benmarouane *et al.*, 2004), and the Williams-Imhof-Matthies-Vinel method (Matthies *et al.*, 1988, 1997; Lutterotti *et al.*, 2004) have been successfully used to describe the texture resulting from packing effects in Bragg-Brentano and Debye-Scherrer powder diffraction measurements using Rietveld refinement programs. The descriptions of the BGMN, DBWS, FULLPROF, GSAS, LHPM, MAUD, and NXD programs and links to them can be obtained via the Collaborative Computational Project, No. 14 (CCP14), http://www.ccp14.ac.uk/. The March and GSH PO models are described in turn below.

A. The March-Dollase PO factor for powder diffraction

The March (1932) model treats the development of PO in a homogeneously deformed medium according to the reorientation of linear and planar indicators. Because deformation is homogeneous, the effect of deformation is to reorient lines and planes. Owen (1973) used a geometrical approach in his development of the model according to the movement of linear markers. This approach has the virtue of avoiding complex tensor mathematics described in the March (1932) paper and of making the deformation more evident. The XRD intensity as a function of orientation for the general case (that is, using a general strain tensor) was derived by Chen (1991),

$$I_j(\theta_j,\phi_j) = \left[S_1^2 \sin^2\theta_j \cos^2\phi_j + \left(\frac{\sin^2\theta_j \sin^2\phi_j}{S_1^2 S_3^2} \right) + S_3^2 \cos^2\theta_j \right]^{-3/2} q, \quad (1)$$

where (θ_j, ϕ_j) are the spherical coordinates, with respect to sample orientation, for the orientation of the goniometer sample stage (Wenk, 1985); S_1 and S_3 are the maximum and

[a)]Also at Research and Development Center, Saudi Aramco, P.O. Box 62, Dhahran 31311, KSA. Electronic mail: sitepu@vt.edu

minimum March stretches, respectively; and q is the XRD intensity of a randomly distributed undeformed sample.

Consider a planar powder diffraction sample formed by a volume conserving cylindrically symmetric compression such that the initial sample thickness d_0 is reduced to d (Dollase, 1986). (Dollase did not include the derivation of the March model at his original paper.) The stretch tensor axial lengths in the sample plane are equal as the sample compression is axially symmetric,

$$S_1 = S_2, \tag{2}$$

and the stretch tensor axial length along the sample normal is defined as the PO parameter r,

$$S_3 = d/d_0 = r. \tag{3}$$

Furthermore, as sample volume is conserved, the product of the stretch tensor axial lengths is unity,

$$S_1 S_2 S_3 = 1. \tag{4}$$

Substitution of Eqs. (2) and (3) into Eq. (4) yields

$$S_1 = S_2 = r^{-1/2}. \tag{5}$$

Substitution of Eqs. (3) and (5) into Eq. (1) gives

$$I_j(\theta_j, \phi_j) = \left[r^{-1} \sin^2 \theta_j \cos^2 \phi_j + \frac{\sin^2 \theta_j \sin^2 \phi_j}{r^{-1} r^2} + r^2 \cos^2 \theta_j \right]^{-3/2} q, \tag{6}$$

which simplifies to

$$I_j(\theta_j, \phi_j) = [r^{-1} \sin^2 \theta_j + r^2 \cos^2 \theta_j]^{-3/2} q \tag{7}$$

or

$$I_j(\theta_j, \phi_j) = P_j q, \tag{8}$$

where

$$P_j = [r^{-1} \sin^2 \theta_j + r^2 \cos^2 \theta_j]^{-3/2} \tag{9}$$

and θ_j is the angle between the PO direction and the reciprocal-lattice vector direction for the Bragg peak that is corrected. The March r parameter controls the distribution shape and is an index of the extent of PO, r being unity for an ideal random-orientation XRD and ND data. For a flat-plate specimen, in which platy crystals pack along the diffraction vector, $r<1$ and needle crystals yield $r>1$. For cylindrical specimens, these relationships are reversed. The March model does not require the use of data acquired with a multiaxis diffractometer for correcting of XRD and ND intensities due to the effects of PO. The model (i) consists of a single r parameter, (ii) is symmetric and smooth across $\theta_j=0°$ and $\theta_j=90°$, (iii) yields a PO correction factor which has either maximum or minimum at $\theta_j=0°$ (see Figure 1), and (iv) is normalizable over the full $2\theta_j$ angular range, i.e.,

$$\int_{\theta_j=0}^{\pi/2} P(\theta_j) \sin(\theta_j) d\theta_j = 1. \tag{10}$$

The normalization is important in that changes in the PO correction factor shape conserve the total intensity within the powder diffraction pattern.

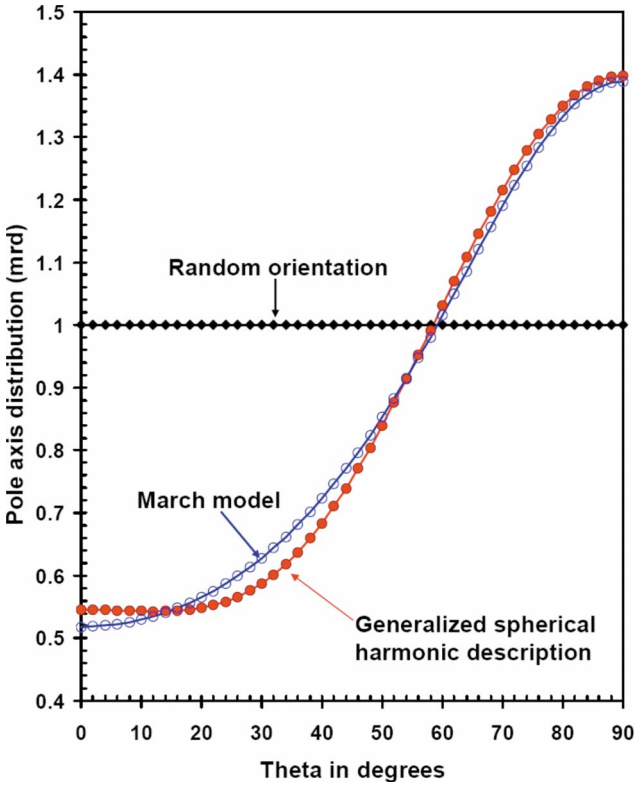

Figure 1. (Color online) The variation of the March PO correction factor with orientation angle. The assumed PO direction for calcite was ⟨001⟩. Pole axial distribution plot for (001) for calcite data derived from Rietveld refinement with GSH description.

B. The GSH texture correction factor

To apply the GSH description, which is generated using selection rules depending on the crystal symmetry of the phase under investigation, the general axis distribution $A(\phi, \beta, \psi, \gamma)$ (Bunge, 1982; Popa, 1992; Von Dreele, 1997) was used,

$$A(\varphi, \beta, \psi, \gamma) = 1 + \sum_{l=2}^{L} \left(\frac{4\pi}{2l+1} \right) \sum_{m=-1}^{+l} \sum_{n=-1}^{+l} C_l^{mn} K_l^m(\varphi, \beta) K_l^n(\psi, \gamma). \tag{11}$$

The two harmonic terms, $K_l^m(\varphi, \beta)$ and $K_l^n(\psi, \gamma)$, take on values according to the crystal and sample symmetries, respectively. These symmetry-modified terms correspond to the angular portions of the atomic orbitals familiar to chemists. Terms with $l=0$ correspond to s orbitals and so are not useful for describing PO. Since diffraction patterns (ignoring the effects of resonant scattering) are centrosymmetric, terms with l odd (which yield noncentrosymmetric orbitals) are not useful for describing PO. Terms with $l=2$ correspond to d orbitals, $l=4$ correspond to g orbitals, etc.

In the diffraction experiment, the crystal (φ, β) and the sample (ψ, γ) coordinates are determined by the choice of reflection index (hkl) and sample orientation on the diffractometer, respectively. The texture is then completely described by the set of C_l^{mn} determined from Rietveld refinement with GSH description. In the case of an ideal random-orientation XRD and ND data, all the harmonic coefficients

are zero, and therefore the general axis distribution is unity (see Figure 1). The magnitude of the texture can be evaluated from the texture index, J, (Bunge, 1982),

$$J = 1 + \sum_{l=2}^{L} \left[\frac{1}{2l+1} \right] \sum_{m=-l}^{l} \sum_{n=-l}^{l} |C_l^{mn}|^2. \quad (12)$$

The objectives of the present study were to characterize the PO and perform crystal structure refinement using ND data collected from uniaxially pressed molybdite and calcite powders. The data were analyzed initially assuming a random orientation of the crystallites and subsequently the PO correction was applied using the March model. The GSH description was independently used as a complementary method to correct the intensities due to the effects of PO. Then, the author compared results and used the model that provided reasonable crystal structure parameters and superior figures of merit to determine crystal structure and phase composition analyses both for (i) cubic and monoclinic phases in annealed solution (850 °C, 15 min) and (ii) cubic, trigonal, monoclinic, and precipitate phases in aged (500 °C, 24 h) polycrystalline Ni-rich $Ni_{50.7}Ti_{49.3}$ shape memory alloy (SMA). ND scattering lengths are -3.44×10^{-15} m for Ti and 10.30×10^{-15} m for Ni, which allow the site occupancies of these two atoms to be refined with far greater reliability than can be achieved with XRD (Sitepu, 2007, 2008).

II. EXPERIMENTAL

A. Molybdite (MoO_3) and calcite ($CaCO_3$) powders and ND data

As a test of the March and GSH PO models, the models were independently used in Rietveld refinements to examine the texture of molybdite and calcite powders. The starting powders were analytical reagents which were supplied by EM Science (USA) and Mallinckrodt Chemical Co. (USA), and their measured neutron pole figures are given in Figure 2. Figure 2 shows that the as-received molybdite powder has stronger PO than the as-received calcite powder. The texture indices for molybdite and calcite are 1.10 and 1.034, respectively. The powders were considered to be excellent for this study because (i) the platy crystallite shapes of molybdite (Calvert *et al.*, 1983; Sitepu, 1991, 1998, 2002) and calcite are consistent with the requirement for the March model that crystallites should be either disk-like or rod-like and (ii) high-quality crystal structures (Kihlborg, 1963; Maslen *et al.*, 1995) have been reported. The other requirement for the March model is that the PO correction factor describing the orientation of crystallites is axially symmetric. This assumption is usually satisfied for uniaxially pressed powder samples and can be ensured by spinning the flat-plate sample about the diffraction vector during data collection.

In the present work, a substantial level of PO was introduced during the specimen preparation. Approximately 2 g of the as-received powder was uniaxially pressed in a cylindrical steel die 1.3 cm in diameter at a pressure of 550 ± 5 MPa. The height of the resulting disk was approximately 0.6 cm. As the relatively weak neutron beam intensity requires the use of large specimens, multiple disks were independently pressed. Five of these disks were then stacked together into a cylinder with a height approximately 3 cm to obtain higher counting rates. The specimens were rotated during the data collection to improve particle statistics.

The ND data were collected at room temperature using the BT-1 32-detector constant-wavelength high-resolution powder diffractometer at the NIST Center for Neutron Research reactor in Gaithersburg, MD, USA. A Cu(311) monochromator with a 90° take-off angle, wavelength of 1.5402 Å, and 15 min incident collimation was employed. Data were collected with counting time approximately 6 h for each sample. The scan range was 10°, with a step size of 0.05°, so that each data point was collected in two adjacent detectors with a total scan range of 3° to 168° 2θ. The data from the 32 detectors were then processed to yield a single histogram using interpolations between adjacent observations to correct for zero-point offsets and detector sensitivities. The BT-1 instrument at NIST Center for Neutron Research is described at http://webster.ncnr.nist.gov/xtal/.

B. Ni-rich $Ni_{50.7}Ti_{49.3}$ SMAs and ND data

It is well known that NiTi SMA combines good functional properties with high strength; therefore, it is recently the most successful shape memory material (Sitepu, Schmahl, Allafi *et al.*, 2002; Sitepu, 2003, 2007; Otsuka and Ren, 2005). There is an interest in Ni-rich NiTi SMAs because the phase transition temperature varies with nickel content. The polycrystalline Ni-rich $Ni_{50.7}Ti_{49.3}$ SMA was annealed at 850 °C for 0.4 h and quenched in water. Figure 3(a) shows the differential scanning calorimeter (DSC) results. This annealed (850 °C, 0.4 h) alloy exhibits a one-step martensitic transformation on both cooling and heating, with DSC peaks at −13 °C on cooling and +14 °C on heating. Subsequently, this annealed alloy was aged at 500 °C for 20 h to promote both the trigonal phase and induce precipitation of Ni_4Ti_3. The aged alloy exhibits a two-step (cubic → trigonal → monoclinic) martensitic transformation on cooling, with DSC peaks at 18 and 7 °C. On heating, a one-step (monoclinic → cubic) transformation with a DSC peak at 43 °C occurs [Figure 3(b)]. [Recently, Sitepu (2007) has shown that on the other two steps (cubic → trigonal → monoclinic) martensitic transformations can also be obtained by adding a small amount of Fe into NiTi alloy, but the precipitate phase did not appear.] There were no changes in the appearance of the DSC curves when experiments were repeated. ND data were measured for (i) the annealed alloy at 38 and −108 °C on cooling and (ii) the aged alloy at 40, 17.8, and −10.2 °C on cooling. ND experiments were performed on cylindrical specimens 0.8 cm in diameter and 7 cm in height, and all experiment details and the ND patterns obtained are given by Sitepu (2008). The ND data were then processed to yield a single diffraction pattern using interpolation between adjacent observations to correct for zero-point offsets and detector sensitivities. The crystal structure of (a) cubic and monoclinic in the annealed (850 °C, 0.4 h) alloy on cooling and (ii) cubic, trigonal, monoclinic, and precipitated Ni_4Ti_3 phases in the aged (500 °C, 24 h) polycrystalline Ni-rich $Ni_{50.7}Ti_{49.3}$ alloy during two-stage phase transformations on cooling were determined using Rietveld refinements with the GSH model.

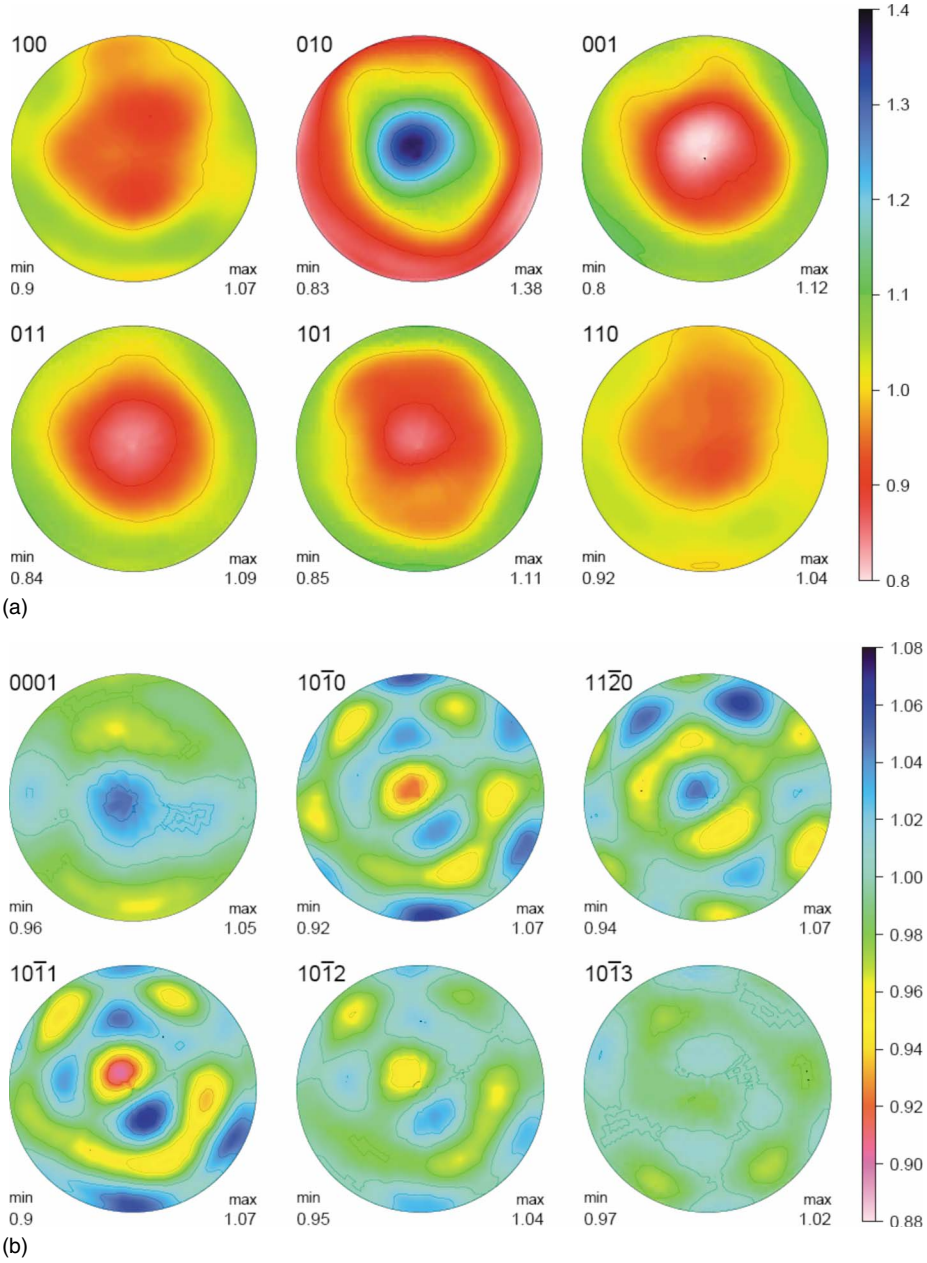

Figure 2. (Color online) (a) The (100), (010), (001), (011), (101), and (110) pole figures for the as-received molybdite powder and (b) the (001), (100), (110), (101), (102), and (103) pole figures for the as-received calcite powders. They are given in equal area projection and linear scale.

C. Rietveld refinement with GSH description

The least-squares structure and profile refinements were performed with GSAS (Larson and Von Dreele, 2000). The structural models used for the molybdite and calcite single-crystal XRD data were described by Kihlborg (1963) and Maslen *et al.* (1995), respectively. The directions of PO used for the ND refinements were ⟨010⟩ for molybdite (Kihlborg, 1963) and ⟨001⟩ for calcite (Sitepu, 1998, 2002). The initial cubic, trigonal, monoclinic, and Ni_4Ti_3 single-crystal structure parameters were taken from Wang, Buehler, and Pickart (1965), Schryver and Potavop (2002), Kudoh *et al.* (1985), and Tirry *et al.* (2006), respectively. The refined parameters were the phase scale factors, the Chebychev polynomial background parameters, the lattice parameters, the instrument zero point, the atomic isotropic and anisotropic displacement coefficients, and the Lorentzian and the Gaussian terms of a pseudo-Voigt profile function. After the preliminary refinement without PO correction ($r=1.00$) had converged, the March PO r parameter was then included. The refinement was carried out with one preferred orientation direction only because with two PO directions and two volume fractions, f (Dollase, 1986), no additional improvements in the figures-of-merits and goodness-of-fit index were obtained (Sitepu *et al.*, 2001, 2005). [GSAS Rietveld software can be used to refine two texture phases, one with March r parameter and volume fraction f and one with March r parameter is unity (random orientation) and volume fraction $(1-f)$. This is the so-called March-Dollase approach in which the parameters r and f are refined.] Subsequently, for Rietveld refinement using GSH description (Sitepu, 2008 and references therein), the default sample texture symmetry was chosen to be cylindrical (or fiber texture) after the preliminary refine-

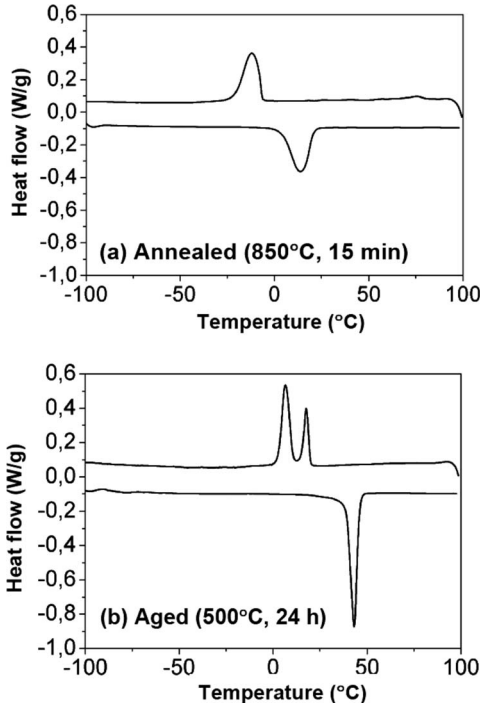

Figure 3. DSC curves for (a) the annealed (850 °C, 0.4 h) and (b) the aged (500 °C, 20 h) Ni-rich $Ti_{49.30}Ni_{50.70}$ SMA.

ment without PO correction had converged. The choice of sample symmetry profoundly affects the selection of harmonic coefficients [see Eq. (11)]. In the case of cylindrical sample symmetry, only $K_l^n(\psi, \gamma)$ terms are zero, so the rest are excluded from the summations, and the set of C_l^{m0} coefficients is sufficient to describe the effect of PO on the ND patterns. The default values for the goniometer angles (ω, χ, and φ) were fixed at (0, 0, and 0). Sixth-order harmonics were selected following preliminary calculations using eight orders that yielded the same figures-of-merit and goodness-of-fit index. Practically, the harmonic order is determined by the magnitude of texture as well as the data quality. Refinements using too many terms diverge and/or yield high-order terms with coefficients insignificantly different from zero.

III. RESULTS AND DISCUSSION

A. Molybdite [MoO_3] and calcite [$CaCO_3$] powders

The as-received molybdite and calcite powders exhibit significant preferred orientation [Figures 2(a) and 2(b)]. The texture indices are 1.10 and 1.03, respectively. The GSH description was used to extract the texture information from a simultaneous refinement with 99 ND patterns Von Dreele and Vogel (2009) held in a variety of orientations in the HIPPO neutron time-of-flight diffractometer at Los Alamos Neutron Scattering Center (LANSCE). So, when additional PO was introduced during the uniaxially pressing of the molybdite and calcite powders, the reliability of the March and GSH PO models could be assessed in correcting intensities for texture.

The refined structural parameters of molybdite (Table I) using either the March model or GSH description agreed quite satisfactorily with the corresponding single-crystal results (Kihlborg, 1963). The figures-of-merit and goodness-of-fit index decreased substantially when the Rietveld refinements were carried out using either the March model or the GSH description. The GSH description provided smaller figures-of-merit and goodness-of-fit index than the March model even if the differences are sometimes small. The texture index [Eq. (12)] for uniaxially pressed molybdite and calcite powders was 1.289, which indicates that the pressed powder has substantially higher texture than that of the as-received specimen as expected.

Reasonable refinements of calcite crystal structure parameters were obtained when applying either the March model or GSH description (Table II). The differences between the present results and those from the synchrotron single-crystal XRD study (Maslen *et al.*, 1995), particularly for some of the anisotropic thermal parameters, probably arise because the calcite sample employed in this study is uniaxially pressed calcite powder at 550 ± 5 MPa. In a study of natural calcite, Von Dreele (1997) noted that only three of the eight anisotropic displacement coefficients obtained by Rietveld refinement agreed well with the single-crystal XRD data (Maslen *et al.*, 1995). Furthermore, an examination of the covariance matrix from the Rietveld refinements showed that there were no significant correlations between the GSH coefficients and the other parameters in the refinements which indicate consistency with the orthogonality properties of harmonic functions. Both the March and the GSH PO models are orthogonal to the refined parameters, such as phase scale factor, zero point, lattice parameters, and the Lorentzian and Gaussian terms of pseudo-Voigt profile function, anisotropic strain parameters (Popa, 1998; Stephens, 1999), structural parameters, and anisotropic thermal parameters for calcite single-crystal synchrotron XRD data (Maslen *et al.*, 1995).

Figure 1 shows typical orientation probability distributions of the uniaxially pressed calcite sample determined by Rietveld refinement with the GSH and March PO models. As expected, the March PO correction factor is maximum at $\theta_j = 90°$ and minimum at $\theta_j = 0°$ when the March r parameter is greater than 1.00. In the case of an ideal random-orientation XRD and ND data, the distribution is unity. The March PO correction factor is slightly lower at the low and high angles than the pole-axis distribution of the ⟨001⟩ uniaxially pressed calcite powder ND data, plotted with the orientation angle φ in Fig. 1 [φ is the angle between the pressing axis and the normal of the (001) calcite plane]. Figure 4 shows the agreement between the calculated and measured ND patterns for uniaxially pressed molybdite and calcite powders at 550 ± 5 MPa following Rietveld refinement with (a) random orientation, (b) the March model, and (c) the GSH models for PO correction. The Rietveld fit obtained from the GSH description is superior to results obtained from the March model (Table II and Figure 4). The generally lower figures-of-merit and goodness-of-fit index obtained from Rietveld refinement using the GSH description may reflect the limitations of the March model with respect to PO correction in the samples examined in the present study and also the larger number of fitted parameters in the GSH model. The GSH description is generally superior and should be used for correction of the PO in ND analysis for both crystal structure refinement and phase composition analysis.

TABLE I. Summary of refined structure parameters, figures-of-merit and goodness-of-fit results, for the uniaxially pressed molybdite [MoO_3] powder at 550 ± 5 MPa obtained from Rietveld refinement. The space group used was *Pbmn* (No. 62). Wyckoff coordinates: $4(c)=x,y,1/4$; $1/2-x,\ 1/2+y,\ 1/4$; $1/2+x,\ 1/2-y,\ 1/4$; and $x,y,3/4$. The isotropic thermal parameters as listed are $B=8\pi^2/U$, where B is the values taken from single-crystal XRD data (Kihlborg, 1963). The Kihlborg values for Mo, O_1, O_2, and O_3 are 0.230(6), 0.561(3), 0.628(4), and 0.951(9), respectively.

	This work				
Parameter	March model	Generalized spherical-harmonic description	Single-crystal XRD data (Kihlborg, 1963)	Δ/σ March	Δ/σ GSH
		Lattice parameters			
a (Å)	3.9624(1)	3.9624(1)	3.9628(7)	−0.6	−0.6
b (Å)	13.860(2)	13.860(2)	13.855(3)	1.4	1.4
c (Å)	3.6971(4)	3.6971(4)	3.6964(6)	1.0	1.0
		Atomic parameters			
Mo($x,y,1/4$)					
x	0.085 03(8)	0.084 90(7)	0.086 69(9)	−13	−15
y	0.101 33(9)	0.101 26(8)	0.101 64(5)	−3.0	−3.8
U	0.006(2)	0.007(2)	0.003(6)	0.5	0.7
$O_1(x,y,1/4)$					
x	0.0348(3)	0.0350(3)	0.0373(9)	−2.6	−2.4
y	0.221 20(10)	0.221 39(9)	0.221 40(4)	−1.8	−0.1
U	0.013(2)	0.013(3)	0.012(9)	0.1	0.1
$O_2(x,y,1/4)$					
x	0.5211(2)	0.5209(2)	0.5212(8)	−0.1	−0.4
y	0.088 07(10)	0.088 28(9)	0.086 57(7)	1.5	1.7
U	0.009(2)	0.010(2)	0.008(4)	0.2	0.4
$O_3(x,y,1/4)$					
x	0.5019(2)	0.5016(2)	0.4994(9)	2.7	2.4
y	0.4361(1)	0.4363(1)	0.435 13(8)	7.5	9.0
U	0.007(2)	0.007(2)	0.007(3)	0	0
		Figures-of-merit and goodness-of-fit index			
R_P	4.99	3.78			
R_{WP}	6.03	4.79			
χ^2	4.31	3.40			
r	1.298(2)	1.000(fixed)			
J	1.000(fixed)	1.269			

B. Crystal structure and phase composition of the annealed (850 °C, 0.4 h) and the aged (500 °C, 24 h) polycrystalline Ni-rich $Ni_{50.7}Ti_{49.3}$ SMAs

The annealed (850 °C, 0.4 h) alloy yields a one-step martensitic transformation on heating and cooling [Figure 3(a)]. Figure 3(b) shows that there are one distinct DSC peak on heating (i.e., monoclinic to cubic phase transformation) and two peaks on cooling (i.e., cubic to monoclinic via trigonal phase transformations) for the aged (500 °C, 24 h) alloy. It is important to highlight that when the aged alloy is investigated at room temperature, it matters whether this temperature was reached by cooling from high temperature to low temperature (i.e., trigonal) or by heating from low temperature to high temperature (i.e., monoclinic). ND patterns of cubic (40 °C), trigonal (17.8 °C), and monoclinic (−10.2 °C) phases are consistent with the DSC results on cooling. Table III reports the refined atomic parameters for high-resolution ND data sets for (i) cubic and monoclinic phases in the annealed-solution $Ni_{50.7}Ti_{49.3}$ alloy and (ii) cubic, trigonal, monoclinic, and precipitate Ni_4Ti_3 in $Ni_{50.7}Ti_{49.3}$ SMA during two-stage phase transformations.

1. Cubic phase

Table III shows structural refinements of cubic phase in both (i) the annealed (850 °C, 0.4 h) alloy and (ii) the aged (850 °C, 24 h) Ni-rich $Ni_{50.7}Ti_{49.30}$ SMA. The crystal structure parameters of Ni_4Ti_3 precipitate phase in the aged $Ni_{50.7}Ti_{49.3}$ SMA are also given in Table III. The results obtained from Rietveld refinement with the GSH description agree reasonably well with the single-crystal XRD data (Wang, Buehler, and Pickart, 1965). The atomic position and isotropic temperature factors for the Ni_4Ti_3 precipitate phase agreed well with the single-crystal results reported by Tirry *et al.* (2006). The annealed (850 °C, 0.4 h) alloy is 100% cubic phase and the aged (850 °C, 24 h) Ni-rich $Ni_{50.7}Ti_{49.30}$ alloy is 93% cubic phase and 7% Ni_4Ti_3. A measured ⟨100⟩ pole figure and orientation distribution function (ODF) for

TABLE II. Summary of Rietveld refinement results for the uniaxially pressed calcite [$CaCO_3$] powder at 550 ± 5 MPa. The space group used was $R\bar{3}c$ (No. 167). Wyckoff coordinates: 6(*c*) are 0,0,0 and 0,0,1/2; 6(*a*) are 0,0,1/4 and 0,0,3/4; and 18(*e*) are $x,0,1/4$; $0,x,1/4$; $-x,-x,1/4$; $-x,0,3/4$; $0,-x,3/4$; and $x,x,3/4$. Cell formula units $Z=6$ and chemical formula weight=100.09.

	This work				
Parameter	March model	Generalized spherical-harmonic description	Single-crystal XRD (Maslen *et al.*, 1995)	Δ/σ March	Δ/σ GSH
		Cell parameters			
a (Å)	4.990 29(14)	4.990 26(14)	4.988(2)	1.1	1.1
c (Å)	17.0687(6)	17.0684(6)	17.068(2)	0.3	0.2
V (Å^3)	368.115(14)	368.103(25)	367.8(3)	0.9	1.0
		Atomic parameters			
O(x,0,1/4)					
x	0.256 67(16)	0.256 44(15)	0.257 00(6)	−1.9	−3.7
		Anisotropic displacement coefficients			
Ca					
U_{11}	0.0174(6)	0.0182(5)	0.009 88(3)	12	17
U_{33}	0.0210(15)	0.0165(14)	0.009 32(4)	7.8	5.1
C					
U_{11}	0.0132(4)	0.0143(4)	0.008 34(9)	12	15
U_{33}	0.0175(12)	0.0171(11)	0.0108(2)	5.6	5.7
O					
U_{11}	0.0172(4)	0.0190(4)	0.011 29(7)	15	19
U_{22}	0.0225(6)	0.0265(6)	0.0220(2)	0.8	7.5
U_{33}	0.0273(8)	0.0258(8)	0.0202(1)	8.9	7.0
U_{13}	−0.003 42(28)	−0.004 12(29)	−0.004 24(6)	2.9	0.4
		Figures-of-merit and goodness-of-fit index			
R_P	5.04	4.66			
R_{WP}	6.59	6.17			
$R(F^2)$	2.92	2.64			
χ^2	4.136	3.637			
r	1.248(4)	1.000(fixed)			
J	1.000(fixed)	1.289			

the cubic phase in the annealed sample are given in Figure 5. The texture data were measured at TEX2, the texture diffractometer at FRG-1, Geesthacht, Germany. Then, the ODFs were calculated using iterative series expansion method, which gives quantitative texture analysis of the sample investigated. While the texture index ($J=1.18$) obtained from Rietveld refinement with GSH description was higher than the expected value of unity for the randomly oriented of materials, the value agrees quite satisfactorily with the corresponding values calculated by the iterative series expansion method. Additionally, the corresponding value for the precipitate is 1.216. It is noted that the texture index of the annealed alloy is slightly higher than that of the aged alloy.

2. Trigonal phase

The refined structure parameters for the trigonal phase agreed reasonably well with the results reported by Sitepu (2007), and the Ni_4Ti_3 precipitate phase in the aged (850 °C, 24 h) Ni-rich $Ni_{50.7}Ti_{49.30}$ SMA also agreed quite well with the single-crystal results of Tirry *et al.* (2006) (Table III). The concentrations of trigonal and precipitate phases are 93% and 7% at room temperature. No significant improvement in the *figures-of-merit* [$R_P, R_{WP}, R(F^2)$] and goodness-of-fit index (χ^2) were found when the inversion center was removed from the $P\bar{3}$ model, suggesting that the space group of trigonal structure in $Ti_{50.75}Ni_{47.75}Fe_{1.50}$ alloy at room temperature, on cooling, was indeed $P\bar{3}$ and not lower symmetry $P3$ or $P31m$. Sitepu (2003, 2007) showed that (i) the refined atomic parameters for all synchrotron diffraction data sets of trigonal phase converged only when the $P\bar{3}$ space group was used in the Rietveld refinement and (ii) a combined neutron and synchrotron refinement confirmed that $P\bar{3}$ is the correct space group for the trigonal phase. While the texture index for the trigonal phase is 1.136, the corresponding value for the precipitate is 1.216 which agrees reasonable with the cubic phase.

3. Monoclinic phase

Kudoh *et al.* (1985) used single-crystal XRD data to determine the monoclinic crystal structure. Subsequently,

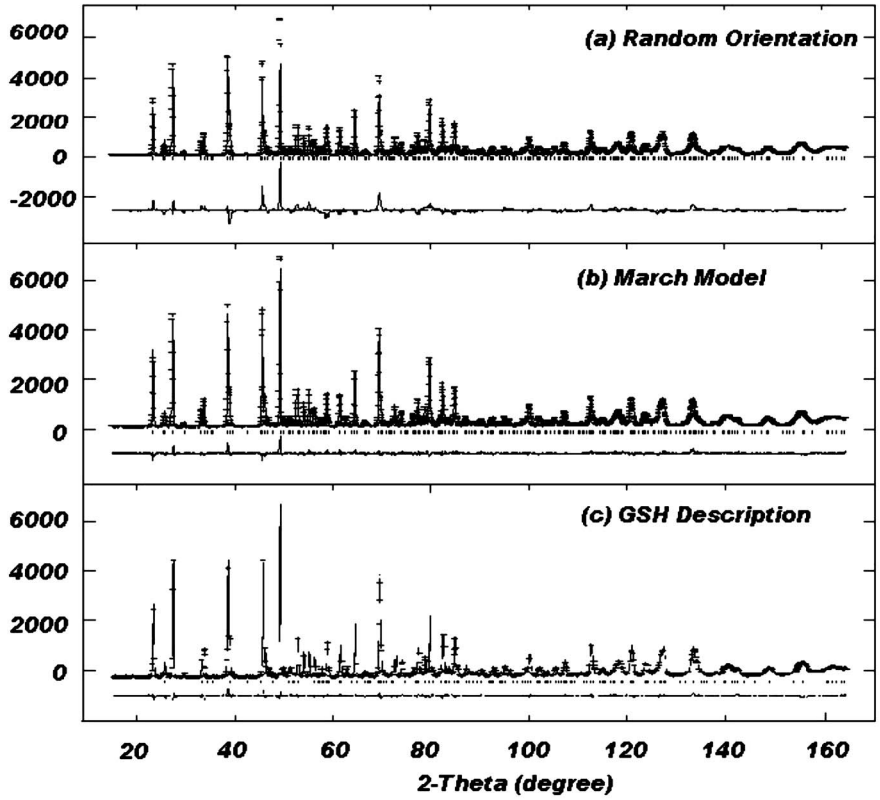

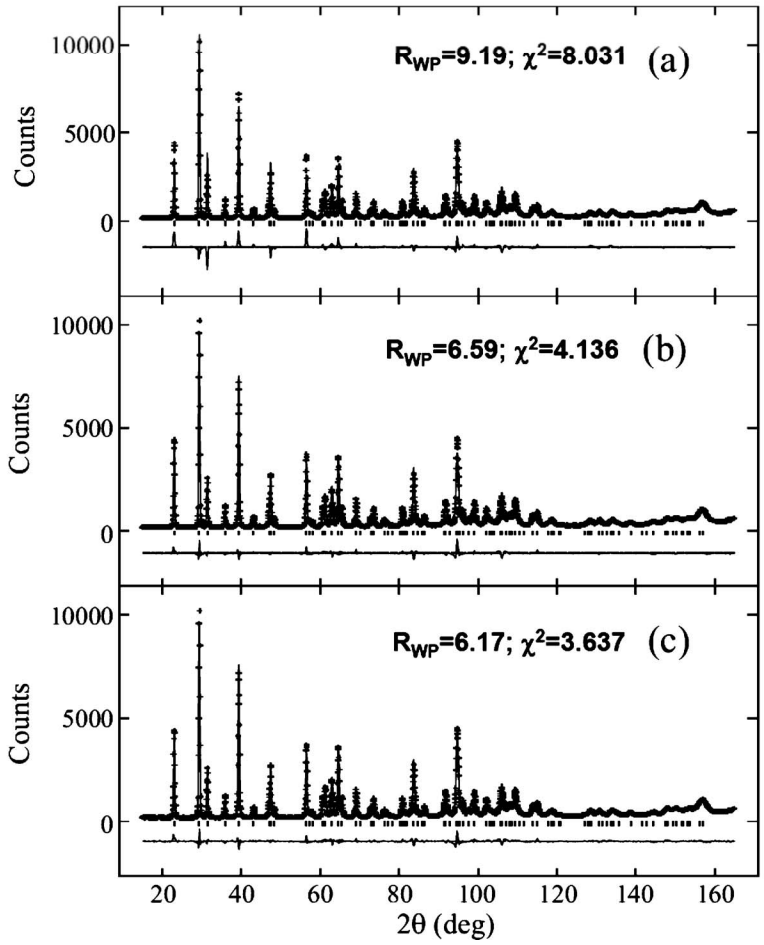

Figure 4. The Rietveld fit for the uniaxially pressed molybdite (top) and calcite (below) powders at 550 ± 5 MPa obtained from (a) the random orientation of the crystallites, (b) the March model, and (c) the GSH models for PO corrections.

TABLE III. Refined crystal structure parameters, figures-of-merit and goodness-of-fit results for the cubic, trigonal, and monoclinic phases in the annealed (850 °C, 0.4 h) and aged (500 °C, 24 h) $Ti_{49.30}Ni_{50.70}$ SMA ND data at -5 ± 7 °C and monoclinic only for ND data at -253 ± 3 °C. The space groups used were $Pm3m$ (No. 221) for cubic, $P112_1/m$ (No. 11) for monoclinic phase, and $P\bar{3}$ (No. 147) for trigonal. Standard deviations in parentheses refer to the last digit. The weight percentage of (i) cubic is 100% for the annealed-solution alloy and (ii) cubic and precipitates are 93% and 7% for the aged alloy.

		Atomic parameters		
			This study	
Refined parameters[a]		Single-crystal XRD data	Annealed	Aged
1. Cubic phase (Wang, Buehler, and Pickart, 1965)				
a (Å)		3.01	3.008 96(11)	3.013 02(8)
Ti(1/2,1/2,1/2)	U_{iso} (Å)^2	N/A	0.004(5)	0.009 54(30)
Ni(0,0,0)	U_{iso} (Å)^2	N/A	0.0329(5)	0.025 96(30)
Precipitate (Ni_4Ti_3) phase $R3R$ (Tirry *et al.*, 2006)				
a (Å)		6.6697(11)		6.720 75(27)
α (deg)		113.838		
Ti(x,y,z)	X	0.4989(10)		0.522(12)
	Y	0.1125(16)		0.093(11)
	Z	0.2513(16)		0.253(14)
	U_{iso} (Å)^2	N/A		0.016(5)
Ni(0,0,0)	U_{iso} (Å)^2	N/A		0.032(5)
Ni(1/2,1/2,1/2)	U_{iso} (Å)^2	N/A		0.032(5)
Ni(x,y,z)	X	0.0605(17)		0.065(7)
	Y	0.5931(11)		0.598(6)
	Z	0.7574(20)		0.762(7)
	U_{iso} (Å)^2	N/A		0.032(5)
Figures-of-merit and goodness-of-fit index				
	R_P	N/A	4.21	4.93
	R_{WP}	N/A	5.33	6.75
	$R(F^2)$	N/A	3.94	26.23
	χ^2	N/A	2.221	2.817
	J_{cubic}	N/A	1.195	1.064
	$J_{precipitate}$	N/A		1.216
2. Trigonal phase (Schryver and Potavop, 2002)				
a (Å)		7.3472(2)		7.341 00(18)
c (Å)		5.2837(3)		5.269 96(27)
Ti(0,0,0)	U_{iso} (Å)^2	N/A		0.0064(10)
Ni(0,0,1/2)	U_{iso} (Å)^2	N/A		0.0155(10)
Ti(x,y,z)	X	0.346		0.341(4)
	Y	−0.02		−0.0067(22)
	Z	0.346		0.3348(27)
	U_{iso} (Å)^2	N/A		0.0064(10)
Ni(x,y,z)	X	0.332		0.3257(16)
	Y	−0.008		−0.0182(8)
	Z	0.815		0.8558(13)
	U_{iso} (Å)^2	N/A		0.0155(10)
Ti(1/3,2/3,z)	Z	0.045		0.023(4)
	U_{iso} (Å)^2	N/A		0.0064(10)
Ni(1/3,2/3,z)	Z	0.547		0.5610(19)
	U_{iso} (Å)^2	N/A		0.0155(10)
Precipitate (Ni_4Ti_3) phase $R3R$ (Tirry *et al.*, 2006)				
a (Å)		6.6697(11)		6.7080(22)
α (deg)		113.838		
Ti(x,y,z)	x	0.4989(10)		0.566(14)
	Y	0.1125(16)		0.099(14)
	U_{iso}	0.2513(16)		0.225(14)
	U_{iso} (Å)^2	N/A		0.020(6)
Ni(0,0,0)	U_{iso} (Å)^2	N/A		0.029(6)

TABLE III. (*Continued.*)

		Atomic parameters		
			This study	
Refined parameters[a]		Single-crystal XRD data	Annealed	Aged
Ni(1/2,1/2,1/2)	U_{iso} (Å)^2	N/A		0.029(6)
Ni(x,y,z)	X	0.0605(17)		0.048(6)
	Y	0.5931(11)		0.587(5)
	Z	0.7574(20)		0.743(6)
	U_{iso} (Å)^2	N/A		0.029(6)
		Figures-of-merit and goodness-of-fit index		
	R_P	N/A		4.89
	R_{WP}	N/A		6.44
	$R(F^2)$	N/A		7.12
	χ^2	N/A		2.360
	$J_{trigonal}$	N/A		1.136
	$J_{precipitate}$	N/A		1.216
		3. Monoclinic phase (Kudoh *et al.*, 1985)		
a (Å)		2.898(1)	2.875 80(32)	2.8894(6)
b (Å)		4.108(2)	4.126 44(34)	4.1334(8)
c (Å)		4.646(3)	4.6325(4)	4.6321(9)
β (deg)		97.78(4)	96.964(7)	96.929(19)
Ti($x,y,1/4$)	x	0.5824(5)	0.594(5)	0.564(5)
	y	0.2836(3)	0.2929(34)	0.2942(35)
	U_{iso} (Å)^2	0.0107	0.033(4)	0.0105(24)
Ni($\bar{x},\bar{y},3/4$)	x	0.0372(4)	0.0334(10)	0.0331(18)
	y	0.1752(2)	0.1760(8)	0.1771(9)
	U_{iso} (Å)^2	0.0126	0.0105(11)	0.0053(12)
		Precipitate (Ni_4Ti_3) phase $R3R$ (Tirry *et al.*, 2006)		
a (Å)		6.6697(11)		6.7211(18)
α (deg)		113.838		
Ti(x,y,z)	x	0.4989(10)		0.567(21)
	y	0.1125(16)		0.172(20)
	z	0.2513(16)		0.299(23)
	U_{iso} (Å)^2	N/A		0.028(7)
Ni(0,0,0)	U_{iso} (Å)^2	N/A		0.030(7)
Ni(1/2,1/2,1/2)	U_{iso} (Å)^2	N/A		0.030(7)
Ni(x,y,z)	x	0.0605(17)		0.060(7)
	y	0.5931(11)		0.609(6)
	z	0.7574(20)		0.760(7)
	U_{iso} (Å)^2	N/A		0.030(7)
		Figures-of-merit and goodness-of-fit index		
	R_P	N/A	4.23	4.92
	R_{WP}	N/A	5.56	6.50
	$R(F^2)$	N/A	3.06	2.75
	χ^2	N/A	2.411	2.440
	$J_{monoclinic}$	N/A	1.098	1.039
	$J_{precipitate}$	N/A		1.221

[a]Wyckoff coordinates: $2(e)=x,y,1/4$ and $2(e)=\bar{x},\bar{y},3/4$ for monoclinic; $1(a)=0,0,0$, $1(b)=0,0,1/2$, $2(d)=1/3,2/3,z$, and $6(g)=x,y,z$ for trigonal.

Sitepu (2008) used Rietveld refinement with GSH description to describe the monoclinic crystal structure of $Ni_{50.14}Fe_{49.86}$ alloy and showed that the refined parameters agree reasonably well with the X-ray single-crystal data. In the present study, the results obtained from Rietveld refinement with the GSH description for ND data of monoclinic phase in (i) annealed-solution (850 °C, 0.4 h) and (ii) aged (850 °C, 24 h) Ni-rich $Ni_{50.7}Ti_{49.30}$ alloys at low temperature

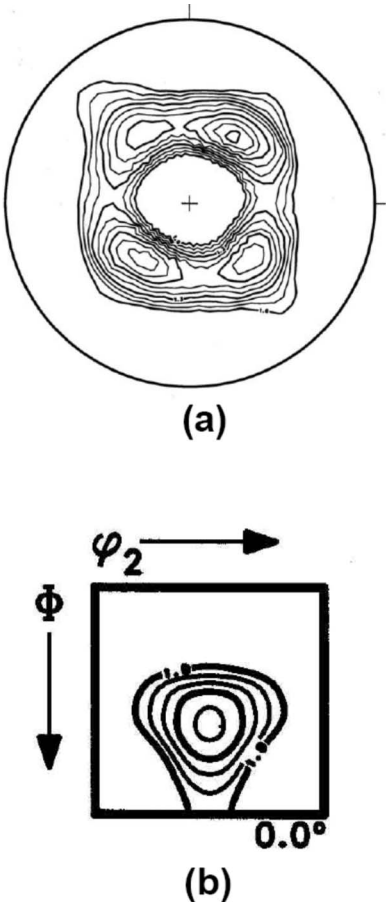

Figure 5. (a) ⟨100⟩ *measured* pole figures for the cubic phase in the annealed $Ti_{49.30}Ni_{50.70}$ SMA with the countour levels of 1.0, 1.1, 1.2, 1.3 1.4, 1.5, 1.6, 1.7, 1.8, and 1.9 multiple of random density (mrd) and the maximum value of pole figure (P_{max}) is 1.9. (b) The ODF of the cubic phase in the annealed $Ti_{49.30}Ni_{50.70}$ alloy with the countour levels of 1.0, 1.2, 1.4 1.6, 1.8, 2.0, and 2.2 mrd and ODF section $\varphi_1=0.0°$. The maximum value of ODF (F_{max}) is 1.9 and φ_1, φ_2, and Φ are Euler angles.

agree quite well with the single-crystal XRD data (Table III). The concentration of Ni_4Ti_3 in the aged (850 °C, 24 h) Ni-rich $Ni_{50.7}Ti_{49.30}$ was 7%. The GSH description can be used successfully to correct the ND intensities due to the effects of PO for the purposes of determining crystal structure information and phase composition analysis of the *two-stage* cubic → trigonal → monoclinic martensitic phase transformations in $Ni_{51.70}Ti_{49.30}$ alloy. The texture indices for the monoclinic and precipitate phases are 1.039 and 1.221. The precipitate has the same texture index for cubic, trigonal, and monoclinic phases. The texture index of the annealed alloy is slightly higher than that of the aged alloy.

IV. CONCLUSIONS

The following conclusion can be drawn:

- ND pole figures of the as-received molybdite and calcite powders showed that the samples have preferred orientation.
- The level of preferred orientation for uniaxially pressured molybdite and calcite powders is higher than the as-received samples.
- The refined structural parameters of uniaxially pressed molybdite and calcite powders obtained from Rietveld refinement with either the March model or GSH description agreed well with the single-crystal results. The GSH description provided a better Rietveld fit than the March model.
- While the annealed alloy has a one-step phase transition on heating and one stage on cooling, the aged alloy shows that there is one-step monoclinic to cubic martensitic transformation on heating and a two-stage cubic → trigonal → monoclinic on cooling.
- The refined atomic parameters obtained from Rietveld refinement with the GSH description for (i) cubic, trigonal, monoclinic, and precipitate (Ni_4Ti_3) phases in the Ni-rich $Ni_{50.7}Ti_{49.3}$ SMA agree reasonably well with the single-crystal XRD data results.
- The GSH description is recommended for correction of the PO in ND analysis for both crystal structure refinement of uniaxially pressed molybdite and calcite powders and phase composition analysis of the annealed-solution and aged Ni-rich $N_{i50.7}T_{i49.3}$ SMA.

ACKNOWLEDGMENTS

The author would like to thank W. A. Dollase for his help in proving the derivation of March model. Also, the author thanks B. H. O'Connor, J. K. Stalick, R. B. Von Dreele, T. Ohba, S. Vogel, K. Otsuka, and H.-G. Brokmeier for their invaluable contributions to the paper. The author is grateful for constructive comments from anonymous reviewers and Associate Editor Dr James Kaduk that help to improve the paper. The author acknowledges the support of the National Institute of Standards and Technology and U.S. Department of Commerce in providing the neutron research facilities used in this work. The work also benefited from the use of the LANSCE, which is funded by the Basic Energy Sciences, Office of Science, U.S. Department of Energy. Thanks to GKSS in Geesthacht, Germany for providing the beam time. The author also acknowledges COMPRES under NSF Cooperative Agreement No. EAR 01-35554 for financial support.

Ahtee, M., Nurmela, M., Suortti, P., and Jarvinen, M. (**1989**). "Correction for preferred orientation in Rietveld refinement," J. Appl. Crystallogr. **22**, 261–268.

Bergmann, J., Monecke, T., and Kleeberg, R. (**2001**). "Alternative algorithm for the correction of preferred orientation in Rietveld analysis," J. Appl. Crystallogr. **34**, 16–19.

Bunge, H. J. (**1982**). *Texture Analysis in Materials Science: Mathematical Methods* (Butterworths-Heinemann, London).

Calvert, L. D., Sirianni, A. F., Gainsford, G. J., and Hubbard, C. R. (**1983**). "A comparison of methods for reducing preferred orientation," Adv. X-Ray Anal. **26**, 105–110.

Chen, T. (**1991**). Ph.D. thesis, University of California.

Dollase, W. A. (**1986**). "Correction of intensities for preferred orientation in powder diffractometry: Application of the March model," J. Appl. Crystallogr. **19**, 267–272.

Järvinen, M. (**1993**). "Application of symmetrized harmonics expansion to correction of the preferred orientation effect," J. Appl. Crystallogr. **26**, 525–531.

Kihlborg, L. (**1963**). "Least squares refinement of the crystal structure of molybdenum trioxide," Ark. Kemi **21**, 357–364.

Kudoh, Y., Tokonami, M., Miyazaki, S., and Otsuka, K. (**1985**). "Crystal structure of the martensite in $Ti_{50.8}Ni_{49.2}$ alloy analyzed by the single crystal X-ray diffraction method," Acta Metall. **33**, 2049–2056.

Larson, A. C. and Von Dreele, R. B. (**2000**). General Structure Analysis System (GSAS), Report LAUR 86-748, Los Alamos National Laboratory, Los Alamos, NM.
Lutterotti, L., Chateigner, D., Ferrari, S., and Ricote, J. (**2004**). "Texture, residual stress and structural analysis of thin films using a combined X-ray analysis," Thin Solid Films **450**, 34–41.
March, A. (**1932**). "Mathematische theorie der regelung nach der korngestalt bei affiner deformation," Z. Kristallogr. **81**, 285–297.
Maslen, E. N., Streltsov, V. A., Streltsova, N. R., and Ishizawa, N. (**1995**). "Electron density and optical anisotropy in rhombohedral carbonates. III. Synchrotron X-ray studies of $CaCO_3$, $MgCO_3$, and $MnCO_3$," Acta Crystallogr., Sect. B: Struct. Sci. **51**, 929–939.
Matthies, S., Lutterotti, L., and Wenk, H.-R. (**1997**). "Advances in texture analysis from diffraction spectra," J. Appl. Crystallogr. **30**, 31–42.
Matthies, S., Wenk, H.-R., and Vinel, G. W. (**1988**). "Some basic concepts of texture analysis and comparison of three methods to calculate orientation distributions from pole figures," J. Appl. Crystallogr. **21**, 285–304.
NIST Center for Neutron Research. ⟨http://webster.ncnr.nist.gov/xtal/⟩.
O'Connor, B. H., Li, D. Y., and Sitepu, H. (**1991**). "Strategies for preferred orientation corrections in X-ray powder diffraction using line intensity ratios," Adv. X-Ray Anal. **34**, 409–415.
O'Connor, B. H., Li, D. Y., and Sitepu, H. (**1992**). "Texture characterization in X-ray powder diffraction using the March formula," Adv. X-Ray Anal. **35**, 277–283.
Otsuka, K. and Ren, X. (**2005**). "Physical metallurgy of Ti-Ni-based shape memory alloys," Prog. Mater. Sci. **50**, 511–678.
Owens, W. H. (**1973**). "Strain modification of angular density distributions," Tectonophysics **16**, 249–261.
Popa, N. C. (**1992**). "Texture in Rietveld refinement," J. Appl. Crystallogr. **25**, 611–616.
Popa, N. C. (**1998**). "The (*hkl*) dependence of diffraction-line broadening caused by strain and size for all Laue groups in Rietveld refinement," J. Appl. Crystallogr. **31**, 176–180.
Rietveld, H. M. (**1969**). "A profile refinement method for nuclear and magnetic structures," J. Appl. Crystallogr. **2**, 65–71.
Schryver, D. and Potavop, P. L. (**2002**) "*R*-phase structure refinement using electron diffraction data," Mater. Trans. **43**, 774–779.
Sitepu, H. (**1991**). MSc thesis, Curtin University of Technology.
Sitepu, H. (**1998**). Ph.D. thesis, Curtin University of Technology.
Sitepu, H. (**2002**). "Assessment of preferred orientation with neutron powder diffraction data," J. Appl. Crystallogr. **35**, 274–277.
Sitepu, H. (**2003**). "Use of synchrotron diffraction data for describing crystal structure and crystallographic phase analysis of *R*-phase NiTi shape memory alloy," Textures Microstruct. **35**, 185–195.
Sitepu, H. (**2007**). "Structural refinement of neutron powder diffraction data of two-stage martensitic phase transformations in $Ti_{50.75}Ni_{47.75}Fe_{1.50}$ shape memory alloy," Powder Diffr. **22**, 209–318.
Sitepu, H. (**2008**). "*In situ* structural and texture analyses of monoclinic phase for polycrystalline Ni-rich $Ti_{49.86}Ni_{50.14}$ alloy from neutron diffraction data," Powder Diffr. **23**, 35–40.
Sitepu, H., O'Connor, B. H., Benmarouane, A., Hansen, T., Ritter, C., and Brokmeier, H.-G. (**2004**). "Texture correction in neutron powder diffraction data of molybdite using the generalized spherical harmonic model," Physica B **350**, e573–e576.
Sitepu, H., O'Connor, B. H., and Li, D. Y. (**2004**). "Deriving the bulk modulus of a single-phase powder from the March preferred orientation parameters," Physica B **350**, e577–e580.
Sitepu, H., O'Connor, B. H., and Li, D. Y. (**2005**). "Comparative evaluation of the March and generalized spherical harmonic preferred orientation models using X-ray diffraction data for molybdite and calcite powders," J. Appl. Crystallogr. **38**, 158–167.
Sitepu, H., Prask, H. J., and Vaudin, M. D. (**2001**). "Texture characterization in X-ray and neutron powder diffraction data using the generalized spherical-harmonic," Adv. X-Ray Anal. **44**, 241–246.
Sitepu, H., Schmahl, W. W., Allafi, J. K., Eggeler, G., Dlouhy, A., Toebbens, D. M., and Tovar, M. (**2002**). "Neutron diffraction phase analysis during thermal cycling of a Ni-rich NiTi shape memory alloy using the Rietveld method," Scr. Mater. **46**, 543–548.
Sitepu, H., Schmahl, W. W., and Stalick, J. K. (**2002**). "Correction of intensities for preferred orientation in neutron-diffraction data of NiTi shape-memory alloy using the generalized spherical-harmonic description," Appl. Phys. A: Mater. Sci. Process. **74**, S1719–S1721.
Sitepu, H., Schmahl, W. W., and Von Dreele, R. B. (**2002**). "Use of the generalized spherical harmonic model for describing crystallographic texture in polycrystalline NiTi shape-memory alloy with time-of-flight neutron powder diffraction data," Appl. Phys. A: Mater. Sci. Process. **74**, S1676–S1678.
Stephens, P. W. (**1999**). "Phenomenological model of anisotropic peak broadening in powder diffraction," J. Appl. Crystallogr. **32**, 281–289.
Tirry, W., Schryvers, D., Jorissen, K., and Lamoen, D. (**2006**). "Electron-diffraction structure refinement of Ni_4Ti_3 precipitates in $Ni_{52}Ti_{48}$," Acta Crystallogr., Sect. B: Struct. Sci. **62**, 966–971.
Von Dreele, R. B. (**1997**). "Quantitative texture analysis by Rietveld refinement," J. Appl. Crystallogr. **30**, 517–525.
Von Dreele, R. B. and Vogel, S. C. (**2009**). Personal communication.
Wang, F. E., Buehler, W. J., and Pickart, S. J. (**1965**). "Crystal structure and a unique "martensitic" transition of TiNi," J. Appl. Phys. **36**, 3232–3239.
Wenk, H. R. (**1985**). *Preferred Orientation in Deformed Metals and Rocks*, edited by Wenk, H.-R. (Academic Press, Orlando), pp. 11–47.